ELSEVIER

NeuroImage

www.elsevier.com/locate/ynimg
NeuroImage 33 (2006) 139 – 153

Human cerebral cortex: A system for the integration of volume- and surface-based representations

Nikos Makris,[a,b,e,f,g,*] Jonathan Kaiser,[a,b,e,f] Christian Haselgrove,[a,b,e,f] Larry J. Seidman,[c,e,f,g] Joseph Biederman,[c,f,g] Denise Boriel,[a,b,e,f] Eve M. Valera,[c,e,f,g] George M. Papadimitriou,[a,b,e,f] Bruce Fischl,[d,e,f,g] Verne S. Caviness Jr.,[a,b,e,f,g] and David N. Kennedy[a,b,d,e,f,g]

[a]*Center for Morphometric Analysis, MGH-East, 149 13th Street, Charlestown, MA 02129, USA*
[b]*Department of Neurology, Boston, MA 02129, USA*
[c]*Department of Psychiatry, Boston, MA 02129, USA*
[d]*NMR Center, Boston, MA 02115, USA*
[e]*A. Martinos Center, Boston, MA 02114, USA*
[f]*Massachusetts General Hospital, Boston, MA 02114, USA*
[g]*Harvard Medical School, Boston, MA 02114, USA*

Received 14 December 2005; revised 3 March 2006; accepted 5 April 2006
Available online 22 August 2006

We describe an MRI-based system for topological analysis followed by measurements of topographic features for the human cerebral cortex that takes as its starting point volumetric segmentation data. This permits interoperation between volume-based and surface-based topographic analysis and extends the functionality of many existing segmentation schemes. We demonstrate the utility of these operations in individual as well as to group analysis. The methodology integrates analyses of cortical segmentation data generated by manual and semi-automated volumetric morphometry routines (such as the program cardviews) with the procedures of the FreeSurfer program to generate a cortical ribbon of the cerebrum and perform cortical topographic measurements (including thickness, surface area and curvature) in individual subjects as well as in subject populations. This system allows the computation of topographical cortical measurements for segmentation data generated from manual and semi-automated volumetric sources other than FreeSurfer. These measurements can be regionally specific and integrated with systems of cortical parcellation that subdivides the neocortex into gyral-based parcellation units (PUs). This system of topographical analysis of the cerebral cortex is consistent with current views of cortical development and neural systems organization of the human and non-human primate brain.

Keywords: Human cerebral cortex; Cortical thickness; Cortical surface area; MRI; Morphometry

Introduction

Measurements of cerebral topographical cortical properties such as thickness, surface area and curvature are of great interest for quantitative normal and clinical investigations of neural development and anatomic connectivity (Carman et al., 1995; Van Essen et al., 1998; Fischl and Dale, 2000). The tangential organization of the cerebral cortex, which gives rise to a topographically unique and architectonic cortical map, is determined by a series of events occurring during neurogenesis (Rakic, 1990b). Cell division in the germinal neuroepithelium and their regulated migration to the cerebral wall results in the formation of a laminated cortical mantle where each neuron has a specific location and, consequently, precise efferent and afferent connections (Rakic, 1972, 1974, 1975; Rakic, 1977; Rakic, 1978, 1982; Purves, 1988; Rakic, 1988, 1990a,b; Caviness et al., 1995; Rakic, 1995; Takahashi et al., 1996a,b). Thickness of the cortex varies from 1 to 5 mm, reaches an average value of 2.5–2.8 mm, and its changes are indicative of changes in the packing density of neurons as well as the content of neuropil (Rockel et al., 1980; Hendry et al., 1987; Jones, 1990).

Cortical thickness is a relatively invariant brain size parameter during mammalian evolution (Prothero and Sundsten, 1984; Mountcastle, 1998). As a matter of fact, neocortical enlargement is principally due to the growth of surface area and only minimally to increases in thickness (Rockel et al., 1980; Hendry et al., 1987; Jones, 1990; Mountcastle, 1998). Cortical surface and brain volume bear a nearly linear relation and the thickness of the cortex remains practically unchangeable for volumes above 3 cm^3 (Hofman, 1989; Mountcastle, 1998). Changes in cortical thickness occur during normal aging as well as in an array of clinical conditions such as Alzheimer's disease, Huntington's disease,

* Corresponding author. Center for Morphometric Analysis, MGH-East, 149 13th Street, Charlestown, MA 02129, USA. Fax: +1 617 7265711.
E-mail address: nikos@cma.mgh.harvard.edu (N. Makris).
Available online on ScienceDirect (www.sciencedirect.com).

1053-8119/$ - see front matter © 2006 Elsevier Inc. All rights reserved.
doi:10.1016/j.neuroimage.2006.04.220

amyotrophic lateral sclerosis and schizophrenia where cortical thinning appears to be regionally specific (Salat et al., 2004; Wiegand et al., 2004; Chung et al., 2005; Gold et al., 2005; Luders et al., 2005c; Narr et al., 2005).

The human cerebral surface has a very complex pattern due to a highly convoluted gyrification, following a pronounced cortical expansion in humans (Brodmann, 1909; Papez, 1929; Igarashi and Kamiya, 1972; Welker, 1990). The trajectory, depth, branching and pattern of the fissures and gyri differ between the two hemispheres of an individual, and it has been suggested that this differentiation is genetically determined (Ono et al., 1990). Although the basic topological pattern of gyri and sulci is maintained across humans, the precise topographic arrangement of each individual gyrus and sulcus shows a high degree of variability between individuals (Dejerine, 1895; Bailey and von Bonin, 1951; Rademacher et al., 1992; Kennedy et al., 1998). This morphological arrangement offers a major challenge for any kind of morphometric analysis whether this is manual or automated (Fischl and Dale, 2000; Luders et al., 2004, 2005a,b).

Surface topographical analyses have been performed automatically by software packages such as FreeSurfer (Dale et al., 1999; Fischl et al., 1999a; Fischl and Dale, 2000) and others (Thompson et al., 1998; Dickson et al., 2001; Kim et al., 2005; Van Essen, 2005). These analyses derive measurements of cortical thickness, surface area and curvature and compute the folding and curvature indices of the surface manifold. Although these analyses are comprehensive for the cerebral cortex, they have not yet been associated with a neural systems anatomical framework that takes into account the topographic specificity of these parameters. The point of this paper is to take advantage of this topographical analysis for segmentation data generated from sources other than FreeSurfer (Filipek et al., 1994; Caviness et al., 1996) and to integrate these analyses within a neural systems biological framework for MRI-based morphometric analysis (Caviness et al., 1999). The vast number of morphometric studies of cerebral cortex has been with a variety of methods such as manual and semi-automated volumetric morphometry, or more recently, voxel-based morphometry (VBM) (Ashburner and Friston, 2000). These studies can now be extended to include cortical thickness, surface area and other topographical measurements. Because each different segmentation methodology has embedded within it, a set of anatomic and operative conventions, it is critical to maintain a constant representation of anatomy between the volumetric and surface-based measures. Specifically, thickness and volume measurements within a given subject optimally should be consistent.

We developed a 'system' to compute topographical cortical measurements for segmentation data generated from manual and semi-automated volumetric sources other than FreeSurfer, including cortical thickness and surface area, in the individual human cortex and to compare these topographical parameters among different populations. We refer to this as a 'system' specifically to distinguish it from a completely new software or methodological development. The 'system' is comprised of existing software frameworks, along with the knowledge of the functional utility and assumptions of the constituent frameworks and the 'glue' algorithms necessary to expand the functionality of these existing software packages. This system is comprehensive and based upon structural MRI scans, topographically specific and allows for integration with other imaging techniques such as morphometric, diffusion tensor MRI (DT-MRI) and functional MRI (fMRI) analyses. We describe here in detail this algorithm and foreshadow its implementation. It is comprised of manual and semi-automated routines of the program cardviews (Caviness et al., 1996) as well as automated procedures that are part of the program FreeSurfer (Dale et al., 1999; Fischl et al., 1999a; Fischl and Dale, 2000). Furthermore, we utilized a gyral-based cortical parcellation framework (Rademacher et al., 1992; Caviness et al., 1996) to define a regionally specific neuroanatomic system for sampling cortical thickness and other surface-based measurements in the cerebrum, and we implemented this method to two example applications. First, it was applied on one individual and second, it was implemented in a group of 18 subjects to determine average global and regional topographical cortical measurements of thickness, surface area, volume and curvature as well as curvature and folding indices. This system of topological cortical surface analysis is consistent with current views of cortical development, connectional and functional organization in the human and non-human primate brain.

Materials and method

Volume constrained analysis of surface topography

Starting from the existence of a voxel-wise segmentation of the cerebral cortex, the system of topographic analysis is executed using the following procedural steps. It should be noted that the system is independent of the method of voxel-based segmentation (i.e., can be applied using methods such as Filipek et al., 1994; Ashburner and Friston, 2000; Smith et al., 2004). After cortical segmentation (Figs. 1A–C), the cortical surface analysis is done using FreeSurfer (Dale et al., 1999; Fischl et al., 1999a; Fischl and Dale, 2000). Using tessellation, a surface is created representing the manually segmented white matter volume. After undergoing smoothing, inflation, and fixing, the process of creating a topologically correct surface, the surfaces can be coregistered, and the exterior surface created allowing for intersubject comparisons of cortical thickness. This will enable the computation of

Fig. 1. Illustration of the topological cortical parcellation (TCP) system. The overall approach is to segment and parcellate the cerebral cortex using cardviews and then use FreeSurfer to compute cortical thickness differences. Panel A shows an intensity normalized T1-weighted MR coronal image. Segmentation (B) and parcellation (C) of the cerebral cortex are executed in the cardviews domain following mainly a manual procedure. The outline files created by the segmentation and parcellation procedures (using cardviews) are converted to a FreeSurfer volume (D for segmentation and E for parcellation). A surface is tessellated (F), smoothed and inflated (G) from the converted FreeSurfer volume. The cortical parcellation map is then overlayed on the inflated surface (1H). An intensity gradient is created throughout the cortex as a function of the distance from the white matter surface according to the manual segmentation of the cerebral cortex (I). The gradient acts as a manufactured T1-weighted MR image from which to place the exterior surface precisely at the location the manual segmentation specifies. The exterior surface is generated by being pushed outward from the white matter surface, following the manufactured gradient to more accurately estimate the CSF/gray surface (J) according to the manual segmentation. With the white and gray surfaces in place, thickness maps are created across the cerebral cortex. The "pial" surface is created using a FreeSurfer algorithm to estimate the pial layer in the cerebral cortex. The white matter surface of each subject is transferred to spherical coordinates and registered to the average MNI brain (K). By registering each subject to a common space each vertex on each subject can be mapped together to allow for intersubject averaging.

cortical topographical measurements such as cortical thickness, curvature, gyrification index, and folding index. Specifically the method is executed in the following five steps, which are elaborated upon below: (1) conversion of cortical segmentation from cardviews to FreeSurfer data format; (2) correction of white matter surface topology; (3) generation of cortex 'gradient' image; (4) generation of exterior surface; and (5) surface registration to a spherical template.

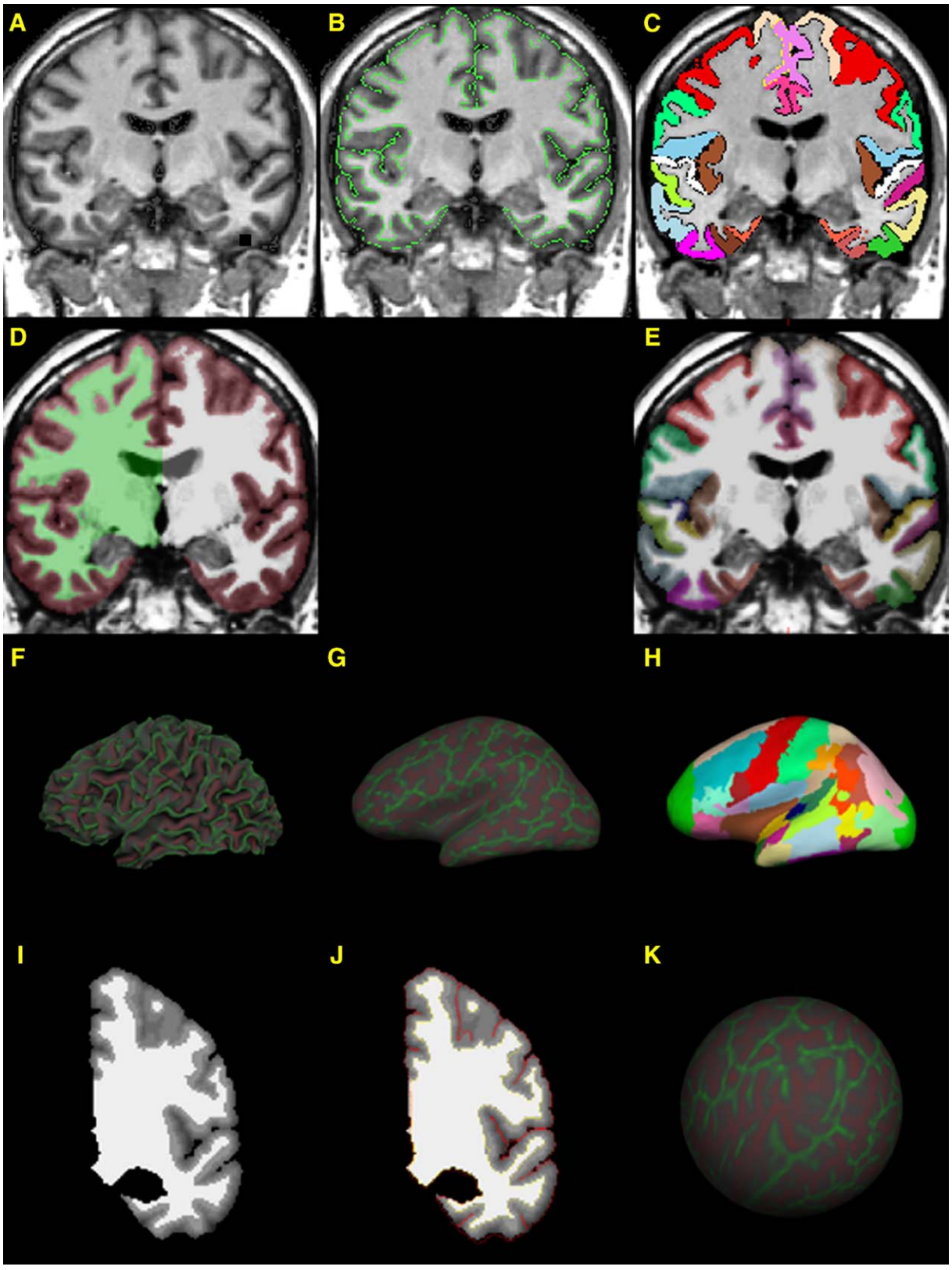

(1) Convert from cardviews to FreeSurfer

In order to utilize the cortical segmentation and parcellation results in the FreeSurfer system, the outline files created by the segmentation are converted to a FreeSurfer volume (Figs. 1D and E). This is done using mri_convert, a program made specifically for the purpose of format conversions.

(2) Topological white matter surface correction

Topological processing requires that the starting surfaces be topologically equivalent to a sphere, free of handles and islands. The surface of the white matter segmentation from the converted volume is tessellated, smoothed, and inflated (Figs. 1F–G). The inherent holes in the surface are filled to be topological correct. The FreeSurfer program mris_fix_topology makes this smoothed and inflated surface.

(3) Cortex gradient

In order to utilize the FreeSurfer exterior finding procedures, an input image must be provided. In the regular mode of FreeSurfer operation, this input image is just the MRI image itself, and an appropriate exterior is found using a built-in set of rules for exterior surface definition. In the case where we have an exterior already defined, the objective is to provide an input image that will induce the processing to find the given exterior. This is effected by generation of an intensity gradient, which is created according to the manual segmentation of the cerebral cortex. The gradient is created throughout the cortex as a function of the distance from the white matter surface (Fig. 1I). The gradient acts as a manufactured T1-weighted MR image from which to place the exterior surface precisely at the location the manual segmentation specifies. A custom algorithm was specifically designed for this purpose.

(4) Exterior surface generation

The exterior surface is generated by an 'outward push' from the white matter surface following the manufactured cortex gradient image until it reaches the exterior csf/gray surface (Fig. 1J) defined by the prior cortical segmentation. With the white and gray surfaces in place, vertex correspondence between the white and exterior surfaces are known and topographic feature (such as thickness, gyrification, curvature, etc.) maps are created for each surface vertex across the cerebral cortex. This process is invoked using the mris_make_surfaces function.

(5) Surface registration

In order to perform intersubject analyses, an individualized standard coordinate system must be adopted. We utilize the spherical coordinate system (Fischl et al., 1999a) for this purpose. The white matter surface of each subject is transferred to spherical coordinates (Fig. 1K) and registered to an atlas. The atlas was initially made from one single subject in the group, and each subject in the dataset was registered to this single subject atlas. Then a final atlas was made by combining each subject's registration to the single subject atlas. By registering each subject to a common space each vertex on each subject can be mapped together to allow for intersubject averaging. This process is invoked using the mris_register function.

Exemplar applications

To demonstrate this system, we make two applications to anatomic analysis data from the archive of volumetric analyses at the Center for Morphometric Analysis at the Massachusetts General Hospital. In Application A, topological cortical parcellation (TCP) was applied in the two hemispheres of one healthy adult human subject. In Application B, a group of eighteen healthy adult subjects were analyzed. These data have already undergone extensive analysis, which is summarized in the next sections.

Magnetic resonance imaging

The analysis was done on magnetic resonance datasets consisting of eighteen normal adult humans. Each subject was scanned on a Siemens Sonata 1.5 T Scanner. The acquisition consisted of a localizer and sagittal T1-weighted images. The volumetric T1-weighted images, which were used for the analysis were as follows: TR=2730 ms, TE=3.39 ms, flip angle=8°, FOV=256 mm, 128 contiguous 1.33 mm slices, matrix=256×256, averages=2.

Image preprocessing—standard orientation and segmentation

The images were resampled into a standard coordinate system based upon the bicommissural line (anterior commissure–posterior commissure) and the interhemispheric fissure (Talairach et al., 1967; Filipek et al., 1988; Talairach and Tournoux, 1988; Filipek et al., 1994). Given this coordinate system, coronal slices were defined perpendicular to the bicommissural line and aligned with the interhemispheric fissure. This positional normalization procedure allowed the reconstruction of a new set of coronal images at the slice thickness of the original acquisition (1.33 mm). The images were not rescaled.

MRI-based segmentation of cerebral cortex and white matter

Neuroanatomic segmentation was performed using semi-automated intensity contour algorithms for external border definition and signal intensity histogram distributions for delineation of gray white borders (Filipek et al., 1994). This technique allows for border definition as the mid-point between the peaks of the bimodal distribution for any given structure and its surrounding tissue (Worth et al., 1997a,b). Segmentation was performed on coronal images and divided the brain into gray matter and white matter regions. The cerebrum was segmented into its principal gray matter and white matter structures and total cerebral white matter. Specifically, the cortical ribbon was defined by two outlines, one external outline between the subarachnoid CSF and the cerebral cortex, and the other between the cerebral cortex and the underlying cerebral white matter (Filipek et al., 1994) as illustrated in Fig. 1B. The total number of voxels in each brain region determined its volume.

Cortical parcellation

The neocortex, which was defined by the aforementioned gray-white matter segmentation procedure, was parcellated further into 48 bilateral parcellation units (PUs) (Rademacher et al., 1992; Caviness et al., 1996) as shown in Fig. 1C. This comprehensive system of cortical parcellation is based upon the configuration of a specified set of cerebral landmarks, mainly neocortical fissures and addresses interindividual topographic variability by preserving the morphological and topographic uniqueness of the individual brain.

The topological cortical parcellation (TCP) system

Use of the system for volume-constrained analysis of surface topography in situations where cerebral cortex is not only

segmented, but contains a parcellation (i.e., subdivision) based upon individualized cortical topology (as implemented, for example, by the methods of Rademacher et al., 1992, Crespo-Facorro et al., 2000), the system can augment volumetric analysis with a comprehensive set of measurements related to the cortical surface topography, specifically of cortical thickness, surface area, curvature as well as folding and curvature indices. Furthermore, it integrates a topographically specific framework of neocortical parcellation, which allows for quantitative analyses in terms of neural systems biology (Caviness et al., 1999). Taking as a starting point a cortical segmentation (Filipek et al., 1994) and parcellation (Caviness et al., 1996), the above system represents the necessary procedures to insert this cortical segmentation into the FreeSurfer processing stream (Dale et al., 1999) for analysis in the surface domain. Figs. 1E and H show the insertion of cortical parcellation in the volume and surface domains, respectively.

Validation of cortical thickness and surface areas

The method for validating the system was to compare the measurements we derived in Application B, focusing on the use of TCP in a group of 18 healthy adult subjects (9 males and 9 females, ages 23–53 years old) with results from published studies of cortical thickness and surface measurements. The majority of these studies were originally generated from postmortem human material. Thus, discrepancies in measurement with our in vivo MRI-based results were anticipated due to the effects of fixation and staining procedures (which take place prior to measurements) on the tissue. The processes that lead to tissue size alteration due to its preparation for histological analyses mainly involve dehydration as well as precipitation of proteins and polymerization. The typical net result of these size changes is tissue shrinkage, with swelling occurring relatively rarely (e.g., Osmium fixation procedures). As has been reported by Braitenberg and Schuz (1998), tissues could show alterations from 42% to 80% of their original volume due to fixation and staining effects (Stephan, 1960; Romeis, 1968; Werner and Winkelmann, 1976; Mouritzen Dam, 1979 O'Kusky and Colonnier, 1982; Drenhaus et al., 1986; Schuz and Palm, 1989). Bearing this caveat in mind, cortical thickness and surface results of classical quantitative studies by Brodmann (1909) and Economo (1927) and more recent studies by Pakkenberg and Gundersen (1997) were utilized for our comparisons. These comparisons pertained primarily to the cortical thickness aspect of our analyses, for which data are more abundant, and secondarily to the surface measurements for which the data were more scarce (Bailey and von Bonin, 1951). The TCP system provides comprehensive data for the cerebral cortex with regional analyses that reach subgyral levels. Thus, comparisons were addressed hierarchically at these different levels. Specifically, the overall cerebral cortical, hemispheric and lobar levels were investigated. At the gyral level of analysis, we targeted our comparisons to cortical areas that both Brodmann and Economo had performed measurements upon. We chose this strategy to ensure consistency given the considerable variability of published results. Since the original cortical data used for this analysis were volumetric in nature and generated by manual segmentation validated in previous studies (Filipek et al., 1994; Caviness et al., 1996), volumetric comparisons with data produced by other methodologies were not included herein.

Results

The system was applied in two separate analyses: Application A, in one individual to evaluate its precision and specificity, and Application B, a group of eighteen normal adult subjects to produce average cortical thickness and other surface topographical measures such as surface area, curvature as well as indices of folding and curvature.

Application A

Topological cortical parcellation (TCP) was applied in the two hemispheres of one healthy adult human subject. In Table 1 and Fig. 2, the regional thickness, surface area, volume, mean curvature, Gaussian curvature, curvature index and folding index of the cortex at the precentral gyrus (PRG) and postcentral gyrus (POG) (which correspond to the primary motor cortex (BA 4) and primary somatosensory cortex (BA 3, 1, 2) respectively), are illustrated and listed. As shown for the left hemisphere in Figs. 2F, G, the thickness of cortical areas varies, and its range can be followed by the aid of a color-coded scheme. This cortical mapping is region specific as shown in Fig. 2E, where a cortical parcellation scheme has been applied on the hemisphere for 48 cortical parcellation units (PUs). In both these applications, the TCP system was used.

Thus, the TCP system provides us with an array of cortical topographical measurements. The definitions of these descriptors

Table 1
The measurements of cortical surface parameters of two representative parcellation units (PUs) are listed in one individual

Cortical region (total)							
Brodmann's area (BA)	Average thickness (SD) (mm)	Surface area (mm^2)	Gray matter volume (mm^3)	Mean curvature (mm^{-1})	Gaussian curvature (mm^{-2})	Folding index	Curvature index
PRG; BA 4 (precentral gyrus)	3.2 (0.7)	11,228	37,783	0.25	0.06	238.25	63.41
POG; BA 3, 1, 2 (postcentral gyrus)	3.0 (0.8)	9107	30,810	0.27	0.07	227.76	55.52

Specifically, these are: the average regional cortical thickness, surface area, volume, mean curvature, Gaussian curvature as well as the curvature index and folding index of the cortex within the precentral gyrus (PRG) and postcentral gyrus (POG) (which correspond to the primary motor cortex (BA 4) and primary somatosensory cortex (BA 3, 1, 2) respectively). In Fig. 2C, this is shown pictorially in a coronal section of the left hemisphere. Abbreviations: CGa: cingulate gyrus, anterior; CO: central operculum; F1: superior frontal gyrus; INS: insula; PHa: parahippocampal gyrus, anterior; POG: postcentral gyrus; PP: planum polare; PRG: precentral gyrus; SMC: supplementary motor cortex; T1a: superior temporal gyrus, anterior; T2a: middle temporal gyrus, anterior; T3a: inferior temporal gyrus, anterior; TFa: temporal fusiform, anterior.

are as follows: surface area is the white matter surface area of the cortical region, calculated by adding the areas of the component triangles of the surface (Fischl and Dale, 2000); gray matter volume is the average of the white matter surface area multiplied by the FreeSurfer-computed cortical thickness integrated across the region and the "pial" surface area multiplied by the cortical thickness integrated across the region (Fischl and Dale, 2000); average thickness is the average of the FreeSurfer-computed thicknesses for each vertex in the region (Fischl and Dale, 2000); mean curvature is the average mean curvature (the average of the principal curvatures at each vertex) for each region; Gaussian curvature is the average Gaussian curvature (the product of the principal curvatures at each vertex) for each region; folding index is the Van Essen folding index for the region (i.e., the integral of the product of the maximum principal curvature and the difference between maximum and minimum curvature divided by 4π) (Van Essen and Drury, 1997); curvature index is the Van Essen curvature index for the region (i.e., the integral across all regions of positive intrinsic curvature divided by 4π) (Van Essen and Drury, 1997). It should be noted that the above cortical topographical measurements computed by the TCP system are not pure FreeSurfer results but are based upon the surfaces created by the manual segmentations and parcellations.

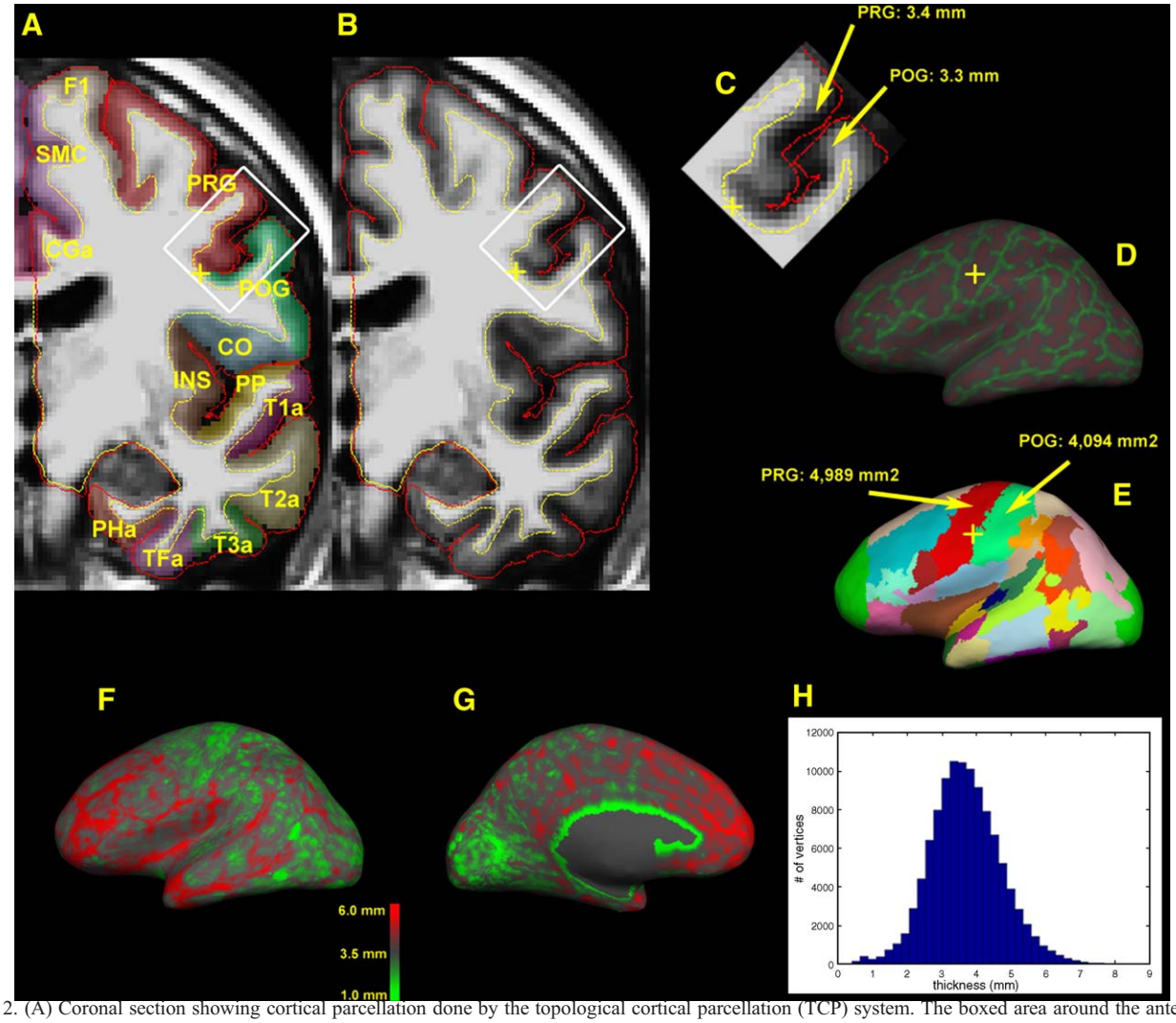

Fig. 2. (A) Coronal section showing cortical parcellation done by the topological cortical parcellation (TCP) system. The boxed area around the anterior and posterior banks of the central sulcus, includes the precentral cortex (PRG) superiorly and the postcentral cortex (POG) inferiorly. The crosshair at the white matter surface in the fundus of the central sulcus indicates the precise topographic correspondence on the lateral surface of the hemisphere on the inflated white matter surfaces shown in panels D and E. (B) Segmentation of the cerebral cortex showing the underlying intensities of the cortex. (C) Detail of cortical region surrounding the central sulcus, which is boxed in panels A and B. It includes the precentral cortex (PRG) and the postcentral cortex (POG). Cortical thickness and surface area values are given in mm and mm^2 respectively for each one of these two cortical regions. (D, E) Lateral view of left hemisphere of the inflated white matter surface. Cross-hair shows the corresponding level of coronal sections A and B. In panel E, the cortical parcellation scheme for 48 cortical parcellation units (PUs) has been superimposed on top of the inflated white matter surface showing the topographic and regional specificity of this cortical mapping. (F, G) Lateral (F) and medial (G) views of the left hemisphere inflated white matter surface with the cortical thickness map of one individual. Red indicates high thickness values, whereas green indicates low thickness values. The range of scale for cortical thickness is from 1 mm to 6 mm. (H) A histogram showing the distribution of thickness across the entire hemisphere. The thickness values are represented in the *X*-axis and the number of vertices on the cerebral surface is indicated on the *Y*-axis.

Application B

A group of eighteen (18) healthy adult subjects were analyzed. The individual estimates of this analysis were then combined across the 18 subjects by using a technique that aligns cortical folding patterns (Fischl et al., 1999b) to produce average cortical thickness and other surface topographical measures and to validate the system for topological cortical parcellation (TCP). Comprehensive measures hierarchically sorted for overall cerebral cortex as well as by hemisphere, lobe and for each of the 48 cortical PUs individually, are contained in Table 2. To validate the thickness measurements, we compared the average cortical thickness values with published data as shown in Table 3a. Similarly, we compared average cortical surface area values with published data, which are shown in Table 3b. Note that there are numerous sources of variance included in this population, including sex and age. A comprehensive evaluation of these biological effects are beyond the scope of this report.

Discussion

The goal of the present study was to make methods for topographical characterization of the cortical mantle more accessible to a broad variety of cortical segmentation techniques. In conjunction with gyral-based cortical parcellation, this system of morphometric analysis and topography provides a spatial framework for identification and measurement of structural changes in the cortex of the living human brain. It draws from existing methodologies of manual, semi-automated and automated procedures of volumetric cortical segmentation and surface topographical analysis. It is therefore able to efficiently apply the strengths of these methodologies to the analysis of volumetric cortical data as well as to group comparison studies (Caviness et al., 1999; Fischl et al., 1999a). Conceptually, this system may be expected to have a number of principal anticipated uses in developmental, cognitive and clinical neuroscience as described below.

Biological implications

First, this system of analysis will provide an MRI-based systemized mapping of normal and pathological neocortical development and topographic ordering of the corticogenetic deployment. Every vertex has a location in the cortical manifold, a distance from other neighboring vertices as well as a thickness and a curvature measurement. Therefore, cortical thickness and curvature at a given location can be expressed as a function of distance. Thus, we can observe a gradient of thickness to determine how it changes in the context of specific hypotheses in developmental neuroscience.

A second utilization will be in testing and mapping anatomical connections in the brain. Cortical thickness provides a correlate of cortical lamination and wiring capacity of a cortical region. Mapping anatomic connectivity will benefit from this system and will allow a fine-grained interrogation of anatomical cortical connections in normal and clinical neuroscience. Cellular architectonics of the mature neocortex is characterized by a vertical distribution of its cells in cortical columns and their horizontal stratification in laminae. The size of these columns ranges from 1 to 2.5 mm^3 allowing them to be sizeable to the voxels currently used in MRI morphometry (Mountcastle, 1998). Cells are linked together by common intrinsic and extrinsic connections within each column and are arranged in six layers or laminae. The thickness of individual cortical layers varies across the cerebral surface depending on the cortical region, ranging from approximately one hundred to several hundreds of micrometers. For instance, in area 17, the thickness of layer II is 90 μm, whereas layer III in area 4 is 1400 μm thick (Economo, 1927; Zilles, 2005). The distribution of neurons in the layers is specific according to growth mechanics and connectional patterns, assigning to each layer a unique pattern of afferent and efferent connections. Generally, neurons within a cortical column give rise to association and commissural fibers from layer III, whereas layers V and VI give rise to subcortical connections with the basal ganglia, thalamus, brainstem, and spinal cord. On the other hand, feedforward input from adjacent cortical regions reaches layers II, III and IV, whereas afferent thalamic and commissural fibers reach layers III and IV (Jones, 1981, 1983; Van Essen et al., 1990; Felleman and Van Essen, 1991). Generally, measurements of regional thickness are indicative of how healthy a cortical area is. For instance, if a set of cortical regions show significant thinning and it is known that those areas are interconnected within a network by specific fiber pathways, then since connections are layer specific and architectonic (Yeterian and Pandya, 1985), it is reasonable to infer that a certain cortical layer and cell type is implicated. This is very powerful information as it could point to directions of cellular and molecular research in disease states or normal aging.

A third domain of use will be in topological measurements of cortical thickness, surface area, volume, curvature, and folding index of regional anatomy providing comprehensive and complete information to elucidate morphogenetic mechanisms of the human brain. Following a series of methodological procedures pertaining to two different streams of analysis (i.e., cardviews and FreeSurfer), which allow the integration of segmentation and surface-based methodologies, a system of topological cortical parcellation (TCP) analysis that is consistent with a wide range of cortical segmentation procedures was created. This system builds upon our experience with topographic segmentation and parcellation of the cerebrum, cerebellum, and brainstem as well as white matter connectivity (Rademacher et al., 1992; Filipek et al., 1994; Caviness et al., 1996; Kennedy et al., 1998; Makris et al., 1999, 2003, 2005 Meyer et al., 1999). Due to their combination with gyral-based cortical parcellation, these topography measures become regionally specific and can be interpreted consistent with current views of corticogenesis, cortical anatomic connectivity and functional organization of the human and non-human primate cerebrum.

Topological cortical measurements using the TCP system

The average cerebral cortical measurements of thickness for the Application B subjects are shown pictorially in Fig. 3. A comprehensive set of regional results for the cortical thickness, surface area and volume, which are listed in Table 2, were in general agreement with our expectations. We had predicted that the cortical thickness values computed by the TCP system would have been close but not necessarily within the range of values derived from each one of the different postmortem analyses. This pattern was observed at different levels of anatomical hierarchy (i.e., the overall cerebral, hemispheric, lobar, and gyral level). More specifically, the overall average cerebral cortical thickness values

Table 2
Master list of average cortical topographical measurements derived from 18 healthy adult humans for the entire cerebral cortex as well as right and left hemispheric cortices separately

	Number of vertices	Surface area (mm^2)	Gray matter volume (mm^3)	Average thickness (mm)	Standard deviation (mm)	Mean curvature (mm^{-1})	Gaussian curvature (mm^{-2})	Folding index	Curvature index
A. Left hemisphere									
Total									
Cerebrum	120,657.1	86,825.3	328,603.8	3.39	0.96	0.27	0.07	2260.53	555.03
Lobes									
Frontal	44,682.5	32,075.1	135,619.1	3.76	0.93	0.26	0.07	829.02	199.76
Parietal	23,400.0	17,030.1	59,370.9	3.22	0.81	0.27	0.07	450.01	109.57
Temporal	26,149.3	18,647.9	72,128.1	3.49	0.92	0.25	0.07	446.20	112.27
Occipital	26,425.3	19,072.3	61,486.2	2.87	0.85	0.28	0.08	535.29	133.43
PU									
AG	1859.8	1371.0	4823.3	3.21	0.65	0.27	0.07	36.22	8.87
CALC	1800.6	1312.7	2553.6	2.07	0.54	0.28	0.08	33.96	8.89
CGa	2365.6	1660.9	6252.9	3.41	1.25	0.26	0.06	45.08	9.75
CGp	2890.8	2044.6	6507.1	3.14	1.07	0.27	0.07	55.98	13.70
CN	788.8	565.6	1709.3	2.94	0.63	0.28	0.08	15.35	3.98
CO	2132.8	1526.8	5249.7	3.49	0.65	0.26	0.07	36.59	9.19
F1	4915.7	3538.5	16,975.9	4.17	0.79	0.25	0.06	82.92	20.67
F2	5362.4	3884.6	16,736.0	3.81	0.74	0.27	0.07	102.11	24.69
F3o	1636.3	1195.7	4605.9	3.51	0.63	0.27	0.07	31.80	7.43
F3t	1218.6	881.6	3555.5	3.68	0.72	0.27	0.07	21.56	5.57
FMC	905.5	649.4	3049.5	4.02	1.01	0.24	0.06	18.37	3.35
FO	773.2	540.8	2107.7	3.73	0.59	0.24	0.05	11.59	2.77
FOC	2855.2	2036.1	8085.4	3.62	0.82	0.26	0.07	52.26	12.94
FP	9395.3	6798.0	34,405.8	4.18	0.86	0.28	0.08	216.31	49.88
H1	693.9	482.3	1571.1	2.92	0.58	0.26	0.07	10.06	3.14
INS	2798.6	1975.9	7177.3	3.95	0.79	0.23	0.06	36.53	10.35
LG	3379.6	2425.3	6704.1	2.58	0.76	0.27	0.08	66.60	16.44
OF	1965.7	1409.4	3463.8	2.44	0.70	0.28	0.08	38.44	9.96
OLi	3359.6	2415.2	8096.0	3.03	0.75	0.28	0.08	63.75	16.37
OLs	7715.4	5576.2	21,609.2	3.30	0.75	0.27	0.07	150.46	36.88
OP	6681.7	4837.8	15,904.5	2.80	0.85	0.30	0.09	151.86	37.10
PAC	2393.6	1699.9	7539.7	4.25	0.72	0.26	0.07	44.50	10.32
PCN	4423.1	3210.4	11,141.1	3.26	0.78	0.28	0.07	87.67	21.55
PHa	1089.5	782.2	3175.8	3.14	1.21	0.28	0.09	33.27	6.12
PHp	653.7	483.8	1488.4	2.72	1.05	0.26	0.07	9.77	2.86
PO	1019.4	743.4	2213.3	3.22	0.55	0.27	0.07	18.48	4.68
POG	6431.3	4729.0	16,295.4	3.06	0.76	0.27	0.07	119.26	28.83
PP	1043.2	717.3	2500.1	3.50	0.67	0.20	0.05	8.93	3.17
PRG	7666.3	5490.4	18,709.1	3.21	0.73	0.25	0.06	115.48	31.08
PT	1537.4	1098.9	3215.6	3.08	0.63	0.25	0.06	21.54	6.09
SC	1616.3	1135.2	4126.5	3.28	1.28	0.24	0.06	29.00	6.38
SCLC	733.9	530.1	1445.4	2.61	0.55	0.28	0.08	14.87	3.80
SGa	2051.2	1492.3	5755.1	3.48	0.76	0.28	0.07	41.71	9.90
SGp	2155.1	1581.0	6123.3	3.43	0.76	0.27	0.07	42.44	10.20
SMC	1445.7	1037.1	4220.1	3.89	0.68	0.25	0.06	21.45	5.74
SPL	2569.2	1858.3	6511.8	3.21	0.67	0.27	0.07	48.24	11.84
T1a	762.9	530.4	2145.6	3.59	0.70	0.24	0.06	11.03	2.98
T1p	1963.3	1414.6	5236.7	3.30	0.74	0.25	0.06	31.49	8.08
T2a	1224.7	870.9	3685.7	3.73	0.80	0.26	0.07	22.20	5.58
T2p	2458.6	1783.7	6998.0	3.49	0.82	0.26	0.07	43.57	10.74
T3a	939.9	665.7	2782.4	3.80	0.77	0.27	0.07	17.11	4.56
T3p	2346.9	1675.5	6858.2	3.61	0.83	0.26	0.07	41.57	10.36
TFa	820.2	584.9	2406.9	3.69	0.83	0.27	0.07	15.68	3.82
TFp	1724.6	1236.3	4332.3	3.31	0.84	0.26	0.07	31.26	7.58
TO2	1375.1	994.6	3697.9	3.36	0.77	0.27	0.07	25.43	6.33
TO3	1098.6	781.5	2832.8	3.19	0.73	0.26	0.07	19.36	4.75
TOF	1254.7	891.3	2623.5	2.82	0.70	0.25	0.06	21.34	5.15
TP	2363.6	1678.2	9399.3	4.12	0.80	0.26	0.07	46.06	10.60

Table 2 (*continued*)

	Number of vertices	Surface area (mm^2)	Gray matter volume (mm^3)	Average thickness (mm)	Standard deviation (mm)	Mean curvature (mm^{-1})	Gaussian curvature (mm^{-2})	Folding index	Curvature index
B. Right hemisphere									
Total									
Cerebrum	122,153.2	87,596.4	325,090.3	3.33	0.96	0.26	0.07	2263.96	557.32
Lobes									
Frontal	45,029.8	32,310.8	135,291.8	3.71	0.93	0.26	0.07	835.14	200.75
Parietal	23,978.2	17,432.2	58,663.5	3.13	0.81	0.27	0.07	458.33	111.35
Temporal	26,343.9	18,686.6	71,661.0	3.45	0.93	0.25	0.07	439.05	112.17
Occipital	26,801.3	19,166.9	59,474.0	2.79	0.80	0.28	0.08	531.44	133.05
PU									
AG	3113.1	2275.3	7626.9	3.12	0.69	0.27	0.07	61.80	14.89
CALC	1952.8	1410.2	2798.5	2.12	0.55	0.28	0.08	38.29	9.83
CGa	2976.5	2104.3	7658.9	3.41	1.18	0.26	0.06	60.78	12.55
CGp	3070.1	2180.1	6484.1	3.00	1.05	0.27	0.07	63.27	14.55
CN	717.2	509.3	1567.8	2.85	0.66	0.28	0.08	14.19	3.60
CO	1879.9	1337.0	4423.6	3.36	0.62	0.26	0.07	29.89	8.11
F1	4517.2	3240.4	15,961.4	4.18	0.79	0.26	0.07	77.99	19.44
F2	4974.1	3597.1	14,743.0	3.71	0.73	0.26	0.07	90.13	21.98
F3o	1928.7	1413.6	5426.0	3.44	0.66	0.27	0.07	36.97	8.84
F3t	1137.7	825.2	3253.9	3.66	0.72	0.26	0.07	19.96	5.02
FMC	999.7	728.3	3446.7	4.08	1.01	0.25	0.06	20.96	3.75
FO	760.4	530.1	2058.5	3.70	0.57	0.23	0.05	11.75	2.79
FOC	2445.9	1741.4	7228.0	3.77	0.81	0.26	0.07	45.56	10.85
FP	10,018.6	7230.1	36,662.5	4.13	0.84	0.28	0.08	229.86	53.31
H1	734.9	510.6	1565.6	2.93	0.58	0.26	0.07	11.11	3.33
INS	2737.8	1939.3	6949.1	3.88	0.80	0.24	0.06	37.69	10.34
LG	3658.4	2613.8	6992.2	2.54	0.74	0.27	0.08	72.82	17.71
OF	1900.3	1356.1	3391.3	2.49	0.68	0.29	0.08	38.41	9.96
OLi	3816.4	2695.5	8547.9	2.86	0.74	0.27	0.08	70.52	18.43
OLs	8236.4	5892.1	21,294.7	3.18	0.73	0.27	0.07	156.60	38.68
OP	5534.1	3984.7	12,956.1	2.76	0.77	0.30	0.09	121.28	29.70
PAC	2552.1	1805.3	7830.4	4.17	0.68	0.25	0.07	43.73	10.98
PCN	4415.1	3177.7	10,861.0	3.22	0.74	0.27	0.07	84.78	21.34
PHa	1141.7	814.8	3477.5	3.32	1.21	0.28	0.09	26.98	6.25
PHp	618.6	454.3	1323.1	2.55	0.94	0.26	0.07	9.03	2.74
PO	822.5	592.8	1658.7	3.15	0.56	0.26	0.07	14.01	3.56
POG	6008.2	4419.0	14,526.3	2.96	0.75	0.27	0.07	108.51	26.75
PP	940.1	637.5	2205.2	3.51	0.65	0.19	0.05	8.07	2.74
PRG	7995.9	5745.2	18,888.8	3.10	0.73	0.25	0.06	122.37	32.31
PT	1218.1	867.4	2583.2	3.11	0.61	0.25	0.06	18.05	4.97
SC	1540.4	1082.3	4126.7	3.35	1.31	0.24	0.06	26.90	5.93
SCLC	985.6	705.3	1925.7	2.62	0.57	0.28	0.08	19.34	5.14
SGa	1272.7	924.9	3662.0	3.41	0.72	0.27	0.07	24.99	5.83
SGp	2783.4	2045.1	7400.2	3.29	0.79	0.27	0.07	53.34	12.88
SMC	1302.6	930.6	3583.5	3.67	0.64	0.24	0.06	18.29	4.89
SPL	2493.0	1817.3	6444.4	3.17	0.67	0.27	0.07	47.63	11.56
T1a	657.8	462.5	2023.8	3.76	0.74	0.24	0.06	10.45	2.62
T1p	2044.1	1461.7	5314.7	3.36	0.71	0.25	0.06	31.01	8.13
T2a	806.7	570.9	2658.4	3.83	0.72	0.26	0.07	14.82	3.56
T2p	2394.9	1724.8	6871.1	3.55	0.83	0.25	0.06	40.36	9.91
T3a	643.7	450.4	1932.3	3.74	0.72	0.26	0.07	11.51	2.90
T3p	2069.7	1460.0	6026.9	3.62	0.84	0.25	0.07	35.32	8.79
TFa	566.0	404.7	1742.7	3.78	0.83	0.27	0.08	11.13	2.77
TFp	1620.0	1152.3	4046.9	3.27	0.78	0.26	0.07	27.73	7.11
TO2	2366.0	1706.1	6064.9	3.32	0.86	0.27	0.07	43.46	10.64
TO3	1866.9	1305.5	4439.7	3.03	0.83	0.25	0.07	30.61	7.95
TOF	1714.8	1201.9	3456.6	2.88	0.74	0.26	0.07	28.71	7.49
TP	2202.2	1561.7	8979.4	4.19	0.82	0.26	0.07	43.01	9.92

(continued on next page)

Table 2 (*continued*)

	Number of vertices	Surface area (mm^2)	Gray matter volume (mm^3)	Average thickness (mm)	Standard deviation (mm)	Mean curvature (mm^{-1})	Gaussian curvature (mm^{-2})	Folding index	Curvature index
C. Whole brain									
Total									
Cerebrum	242,810.3	174,421.7	653,694.1	3.36	0.96	0.27	0.07	4524.49	1112.36
Lobes									
Frontal	89,712.3	64,385.9	270,910.9	3.73	0.93	0.26	0.07	1664.16	400.52
Parietal	47,378.2	34,462.2	118,034.4	3.17	0.81	0.27	0.07	908.34	220.93
Temporal	52,493.3	37,334.6	143,789.1	3.47	0.92	0.25	0.07	885.25	224.44
Occipital	53,226.6	38,239.2	120,960.2	2.83	0.82	0.28	0.08	1066.74	266.47
PU									
AG	4972.9	3646.3	12,450.3	3.15	0.67	0.27	0.07	98.03	23.76
CALC	3753.4	2722.9	5352.1	2.10	0.54	0.28	0.08	72.25	18.72
CGa	5342.1	3765.3	13,911.8	3.41	1.21	0.26	0.06	105.86	22.30
CGp	5960.9	4224.7	12,991.2	3.07	1.06	0.27	0.07	119.25	28.25
CN	1506.1	1074.9	3277.1	2.90	0.65	0.28	0.08	29.54	7.58
CO	4012.7	2863.8	9673.3	3.43	0.64	0.26	0.07	66.48	17.30
F1	9432.9	6778.9	32,937.3	4.17	0.79	0.25	0.07	160.91	40.12
F2	10,336.5	7481.6	31,479.0	3.76	0.73	0.26	0.07	192.24	46.67
F3o	3565.0	2609.3	10,031.9	3.47	0.64	0.27	0.07	68.77	16.27
F3t	2356.3	1706.8	6809.4	3.67	0.72	0.26	0.07	41.52	10.59
FMC	1905.2	1377.8	6496.2	4.05	1.01	0.24	0.06	39.33	7.10
FO	1533.6	1070.9	4166.2	3.72	0.58	0.23	0.05	23.34	5.56
FOC	5301.2	3777.5	15,313.4	3.69	0.82	0.26	0.07	97.83	23.80
FP	19,413.9	14,028.1	71,068.3	4.15	0.85	0.28	0.08	446.17	103.19
H1	1428.8	992.9	3136.7	2.93	0.58	0.26	0.07	21.17	6.47
INS	5536.4	3915.2	14,126.4	3.91	0.80	0.24	0.06	74.22	20.69
LG	7038.1	5039.1	13,696.2	2.56	0.75	0.27	0.08	139.42	34.15
OF	3866.0	2765.5	6855.1	2.47	0.69	0.28	0.08	76.86	19.92
OLi	7176.0	5110.7	16,643.9	2.94	0.74	0.27	0.08	134.27	34.80
OLs	15,951.8	11,468.3	42,903.9	3.24	0.74	0.27	0.07	307.06	75.56
OP	12,215.7	8822.4	28,860.6	2.78	0.81	0.30	0.09	273.14	66.80
PAC	4945.7	3505.2	15,370.2	4.21	0.70	0.26	0.07	88.23	21.30
PCN	8838.2	6388.1	22,002.1	3.24	0.76	0.28	0.07	172.45	42.89
PHa	2231.2	1597.1	6653.3	3.23	1.21	0.28	0.09	60.25	12.37
PHp	1272.2	938.2	2811.4	2.64	1.00	0.26	0.07	18.80	5.60
PO	1841.9	1336.2	3871.9	3.19	0.56	0.27	0.07	32.49	8.24
POG	12,439.6	9148.0	30,821.7	3.01	0.75	0.27	0.07	227.77	55.58
PP	1983.2	1354.8	4705.3	3.50	0.66	0.20	0.05	17.00	5.91
PRG	15,662.2	11,235.6	37,597.9	3.15	0.73	0.25	0.06	237.85	63.39
PT	2755.5	1966.3	5798.8	3.09	0.62	0.25	0.06	39.60	11.07
SC	3156.8	2217.6	8253.2	3.32	1.30	0.24	0.06	55.90	12.31
SCLC	1719.6	1235.4	3371.2	2.62	0.56	0.28	0.08	34.20	8.94
SGa	3323.9	2417.2	9417.1	3.46	0.74	0.27	0.07	66.70	15.73
SGp	4938.5	3626.1	13,523.5	3.35	0.78	0.27	0.07	95.78	23.08
SMC	2748.2	1967.7	7803.6	3.79	0.66	0.25	0.06	39.75	10.63
SPL	5062.2	3675.6	12,956.2	3.19	0.67	0.27	0.07	95.87	23.40
T1a	1420.7	992.9	4169.4	3.67	0.72	0.24	0.06	21.48	5.60
T1p	4007.4	2876.3	10,551.4	3.33	0.73	0.25	0.06	62.50	16.21
T2a	2031.4	1441.9	6344.1	3.77	0.77	0.26	0.07	37.02	9.15
T2p	4853.5	3508.5	13,869.1	3.52	0.83	0.26	0.07	83.93	20.65
T3a	1583.7	1116.1	4714.7	3.78	0.75	0.27	0.07	28.62	7.46
T3p	4416.6	3135.5	12,885.1	3.62	0.83	0.25	0.07	76.89	19.15
TFa	1386.2	989.6	4149.6	3.72	0.83	0.27	0.07	26.81	6.60
TFp	3344.6	2388.6	8379.2	3.29	0.81	0.26	0.07	58.99	14.69
TO2	3741.1	2700.7	9762.8	3.33	0.83	0.27	0.07	68.89	16.96
TO3	2965.6	2087.0	7272.5	3.09	0.80	0.25	0.07	49.97	12.71
TOF	2969.5	2093.2	6080.1	2.86	0.72	0.25	0.06	50.05	12.64
TP	4565.8	3239.9	18,378.7	4.15	0.81	0.26	0.07	89.07	20.52

Table 3a
Comparisons of the average cortical thickness (3a) and surface area (3b) measurements derived by the topological cortical parcellation (TCP) system with reported postmortem analyses

Cortical region (total); Brodmann's area (BA)	Brodmann (1909); postmortem thickness (mm)	Economo (1927); postmortem thickness (mm)	Pakkenberg and Gundersen (1997); postmortem thickness (mm)	CTP; average ($n=18$) In vivo thickness (mm)
Overall average	1.5–4.5	1–4.5	2.7	3.36
Frontal lobe	–	1–4.5	2.8	3.73
Parietal lobe	–	1.9–3.6	2.6	3.17
Temporal lobe	–	2.7–3.8	2.8	3.47
Occipital lobe	–	1.8–2.6	2.2	2.83
Precentral gyrus; BA 4; PRG	3.0–4.5	3.5–4.5	–	3.15
Calcarine region; BA 17; CALC and SCLC	2.3–2.6	1.8–2.2	–	2.26
Precuneus and Superior Parietal Lobule; BA 7; PCN and SPL	3.1	2.8–3.0	–	3.22
Parahippocampal gyrus; BA 28; PHa and PHp	2.3	2.7	–	3.02
Supplementary motor cortex; BA 6; SMC	3.0–3.8	3.2–4.0	–	3.79

For cortical thickness, the overall cerebral cortical, hemispheric and lobar levels were investigated. At the gyral level of analysis, we targeted the comparison of cortical thickness measurements for cortical areas that both Brodmann and Economo had analyzed in postmortem material (3a). For surface area instead (due to scarcity of published postmortem data), comparisons were done only at the overall cerebral cortical level (3b).

by TCP was 3.36 mm, which falls within the range of the observations by Brodmann (1909) (1.5–4.5 mm) and Economo (1927) (1–4.5 mm). In contrast, it was above the highest value of the findings of Pakkenberg and Gundersen (1997) by 0.66 mm. At the lobar level, the TCP results fell within the range of the observations by Economo (1927) for the frontal, parietal and temporal lobes; however, the occipital lobe fell off range by 0.23 mm from Economo's highest value. Pakkenberg and Gundersen's results were lower in a systematic fashion. Furthermore, the results of this procedure showed, consistent with published findings (Economo, 1927) that, throughout the cerebrum, the cortex at the crown of a gyrus was thicker than at the fundus of the sulcus, which constitutes the floor of that gyrus. Specifically, the overall average cerebral cortical thickness measurement at the crowns was 3.44 mm contrasted to the fundi that was 3.3 mm. Moreover, additional relationships of gyral cortical thickness, as observed by Brodmann (1909), were consistent with the results of the TCP system. Specifically, the cortex of the precentral gyrus (PRG, BA 4) was thicker than that of the calcarine cortex (CALC and SCLC, BA 17) and the parahippocampal cortex (PHa and PHp, BA 28,29, 30) was thicker than the calcarine cortex (BA 17) and thinner than the cortex of the precentral gyrus (BA 4). In the TCP system results the thickness of these areas were as follows: PRG was 3.15 mm, PH (weighted average of vertices of PHa and PHp) was 3.02 mm and the calcarine cortex (weighted average of vertices of CALC and SCLC) was 2.26 mm. Thus the findings derived by the TCP system on cortical thickness relationships were consistent with Brodmann's original observations. The overall cerebral cortical surface area results by the TCP system, as shown in Table 3b, were in agreement with the literature findings published by Pakkenberg and Gundersen (1997). Bailey and von Bonin (1951) and Economo (1927) reported results with higher values for overall cerebral cortical surface area measurement. Moreover, all of these measurements of cortical topography (i.e., cortical thickness and surface area as well as mean curvature, Gaussian curvature, folding index and curvature index) can be used to characterize geometric differences between groups of subjects.

Multimodal imaging

When cortical thickness measurements are combined with data generated by other imaging modalities such as DT-MRI or fMRI, they can allow drawing inferences of specific laminar alterations. For example, if there is a combined observation of alterations in cortical thickness of multimodal association areas and fractional anisotropy (FA), volumetric or tractographic changes of long corticocortical association fiber tracts known to interconnect the damaged cortical regions, then layer III could be altered. Similarly, if volumetric or VBM-based alterations are encountered in a thalamic region as well as thickness changes in a cortical area

Notes to Table 2.
These comprehensive measures are hierarchically sorted for overall cerebral cortex as well as by hemisphere, lobe and for each of the 48 cortical parcellation units (PUs) individually. Abbreviations: AG: angular gyrus; CALC: intracalcarine cortex; CGa: cingulate gyrus, anterior; CGp: cingulate gyrus, posterior; CN: cuneal cortex; CO: central operculum; F1: superior frontal gyrus; F2: middle frontal gyrus; F3o: inferior frontal gyrus, pars opercularis; F3t: inferior frontal gyrus, pars triangularis; FMC: frontal medial cortex; FO: frontal operculum; FOC: frontal orbital cortex; FP: frontal pole; H1: Heschl's gyrus; INS: insula; LG: lingual gyrus; OP: occipital pole; OF: occipital fusiform gyrus; OLi: lateral occipital cortex, inferior; OLs: lateral occipital cortex, superior; PAC: paracingulate cortex; PCN: precuneus; PHa: parahippocampal gyrus, anterior; PHp: parahippocampal gyrus, posterior; PO: parietal operculum; POG: postcentral gyrus; PP: planum polare; PRG: precentral gyrus; PT: planum temporale; SC: subcallosal cortex; SCLC: supracalcarine cortex; SGa: supramarginal gyrus, anterior; SGp: supramarginal gyrus, posterior; SMC: supplementary motor cortex; SPL: superior parietal lobule; T1a: superior temporal gyrus, anterior; T1p: superior temporal gyrus, posterior; T2a: middle temporal gyrus, anterior; T2p: middle temporal gyrus, posterior; T3a: inferior temporal gyrus, anterior; T3p: inferior temporal gyrus, posterior; TFa: temporal fusiform, anterior; TFp: temporal fusiform, posterior; TO2: middle temporal gyrus, temporooccipital; TO3: inferior temporal gyrus, temporooccipital; TOF: temporooccipital fusiform gyrus; TP: temporal pole.

Table 3b

Cortical region	Economo (1927); postmortem surface area (mm^2)	Bailey and Bonin (1951); postmortem surface area (mm^2)	Pakkenberg and Gundersen (1997); postmortem surface area (mm^2)	CTP; average ($n=18$) in vivo surface area (mm^2)
Overall average	220,000	187,700–243,800	168,000–190,000	174,421

connected to this part of the thalamus, then it is logical to infer that layers V and VI would be implicated. Moreover, if fMRI alterations such as signal decrease are observed in cortical regions where measurements show a decrease in thickness, then that dysfunction could be associated with a structural alteration of that cortical area.

Integrability of data

Data generated by a diversity of modalities describing different brain characteristics need to be integrated into a common coordinate space to give a holistic representation of the brain under investigation as well as to understand differences between individuals and populations. It is important that computational models investigating variability of structure, especially neocortex (which has the highest degree of error readily observable when mapping into a common database or coordinate system), although allowing variations in interpretations, should be able to integrate the data. In this context, the ability of morphometric volumetric data and surface data to interact becomes of particular interest given that the surface characteristics of the individual cerebrum have to be taken into account precisely. Currently, it is uncertain how to address this question satisfactorily using computational atlases, since these atlases blur the distortion between databases and traditional atlases (Toga, 2002). The TCP system capturing such current modular package designs as FreeSurfer is interoperable within an integrated processing environment.

Limitations

The quality of analyses derived from this cortical topological method will be comparable to the quality of imaging data that are

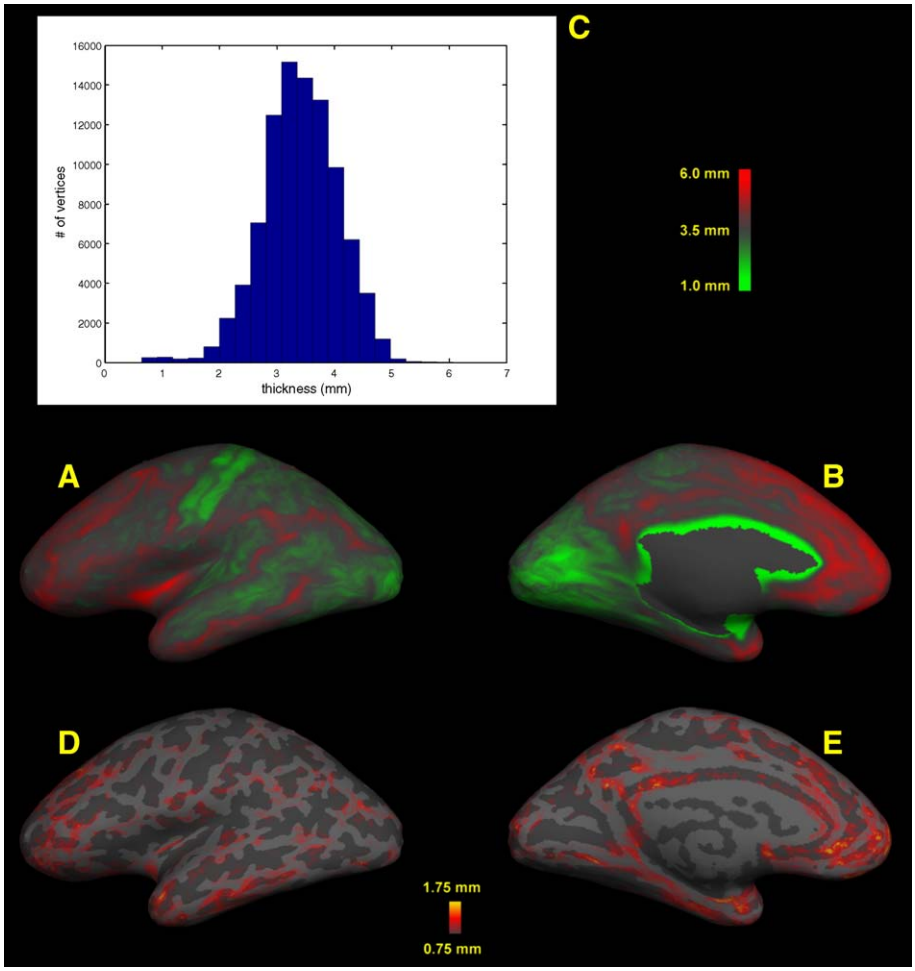

Fig. 3. Lateral (A) and medial (B) views of the left hemisphere inflated white matter surface with the average cortical thickness map of 18 individuals. Red indicates high thickness values, whereas green indicates low thickness values. The range of scale for cortical thickness is shown in the colored bar. In panel C, a histogram is showing the distribution of thickness across the entire hemisphere. The thickness values are represented in the *X*-axis and the number of vertices on the cerebral surface is indicated on the *Y*-axis. In the lateral (D) and medial (E) inflated white matter surfaces of the left hemisphere, the map of standard deviations of the cortical thickness measurements across 18 subjects is shown. Subcortical regions in the medial aspect of the surface have been excluded. Areas showing higher thickness variation are colored in yellow and red.

analyzed. Thus, quality of segmentation is essential. Entry into the surface-based domain of analysis requires attention to the topology of the underlying white matter structure. Most segmentation tools performing voxel-based labeling do not explicitly constrain the topology of the result. Similarly, three-dimensional continuity of segmentation is critical for accurate surface-based calculations. The thickness and curvature measures can be substantially altered by these segmentation factors.

The effective resolution of any system for the interrogation of cortical structure is dependent upon many factors, and these factors have a dramatic effect on the classes of inference that can be drawn from the data. Scales of interest can range from lobes, to gyri, cytoarchitecture and ultimately to the cortical column. A primary limiting factor is that of the initial imaging resolution. Secondarily, the original voxel-representation of imaged values are transformed into a surface tessellation. In the data demonstrated here, the average surface area of the triangle defined by three adjacent vertices is approximately 0.35 mm^2. Given that the surface magnitude of an average cortical column is 0.50 mm^2, it will allow approximately one and a half triangles to fit within the surface area of a cortical column. However, effective real columnar resolution will require advances in acquisition resolution and registration techniques to develop techniques that account for the requisite anatomic variations. Ultimately, when this effective resolution can be obtained, such developmental questions can be addressed as to whether or not developmental changes in cortical thickness are continuous functions at an unprecedented spatial scale. This can be investigated within a given cytoarchitectonic field and between fields.

Conclusions

A system of topographic analysis that integrates volume- and surface-based techniques is described and demonstrated. Application of this system can be envisioned, which include procedures of MRI-based anatomical manual and semi-automated segmentation (Filipek et al., 1994) or voxel-based morphometry (VBM) (Ashburner and Friston, 2000) and cortical parcellation (Caviness et al., 1996) as well as computational methods of constructing (Dale et al., 1999; Fischl et al., 1999a) and transforming (Fischl et al., 1999a) models of the cerebral cortex, and an intersubject alignment procedure (Fischl et al., 1999b). This system allows the computation of topographical cortical measurements for segmentation data generated from manual and semi-automated volumetric sources other than FreeSurfer, including cortical thickness and surface area, in the individual human cortex and to compare these topographical parameters among different populations. We anticipate that these new techniques, which are integrable with other imaging modalities, will advance our knowledge of brain development, aging and its organization in normal conditions and in disease.

Acknowledgments

Preparation of this article was supported in part by grants from The National Association for Research in Schizophrenia and Depression (NARSAD) and the National Institutes of Health National Center for Complementary and Alternative Medicine NCAM (NM); the Fairway Trust (DK); NIMH MH/HD 62152 (LJS), the March of Dimes Foundation (LJS) and the Mental Illness and Neuroscience Discovery (MIND) Institute (LJS); National Research Service Award (NIMH F32 MH065040-01A1), Peter Livingston Fellowship through the Harvard Medical School Department of Psychiatry, and the Clinical Research Training Program Fellowship in Biological and Social Psychiatry MH-16259 (EMV); NIMH MH 57934 (Steve Faraone), the NARSAD Distinguished Investigator Award (JB), the Janssen Pharmaceuticals and the Johnson and Johnson Center for the Study of Psychopathology (JB); The National Center for Research Resources (P41RR14075).

References

Ashburner, J., Friston, K.J., 2000. Voxel-based morphometry—The methods. NeuroImage 11, 805–821.

Bailey, P., von Bonin, G., 1951. The Isocortex of Man. University of Illinois Press, Urbana.

Braitenberg, V., Schuz, A., 1998. Statistics and Geometry of Neuronal Connectivity. Springer, Heidelberg.

Brodmann, K., 1909. Vergleichende Lokalisationslehre der Grosshirnrinde. Verlag von Johann Ambrosius Barth, Leipzig.

Carman, G.J., Drury, H.A., Van Essen, D.C., 1995. Computational methods for reconstructing and unfolding the cerebral cortex. Cereb. Cortex 5, 506–517.

Caviness, V.S.J., Kennedy, D.N., Bates, J., Makris, N., 1995. Advanced application of magnetic resonance imaging in human brain science. Brain Dev. 17, 399–408.

Caviness, V.S.J., Makris, N., Meyer, J., Kennedy, D., 1996. MRI-based parcellation of human neocortex: an anatomically specified method with estimate of reliability. J. Cogn. Neurosci. 8, 566–588.

Caviness Jr., V.S., Lange, N.T., Makris, N., Herbert, M.R., Kennedy, D.N., 1999. MRI-based brain volumetrics: emergence of a developmental brain science. Brain Dev. 21, 289–295.

Chung, M.K., Robbins, S.M., Dalton, K.M., Davidson, R.J., Alexander, A.L., Evans, A.C., 2005. Cortical thickness analysis in autism with heat kernel smoothing. NeuroImage 25, 1256–1265.

Crespo-Facorro, B., Kim, J., Andreasen, N.C., Spinks, R., O'Leary, D.S., Bockholt, H.J., Harris, G., Magnotta, V.A., 2000. Cerebral cortex: a topographic segmentation method using magnetic resonance imaging. Psychiatry Res. 100, 97–126.

Dale, A.M., Fischl, B., Sereno, M.I., 1999. Cortical surface-based analysis: I. Segmentation and surface reconstruction. NeuroImage 9, 179–194.

Dejerine, J., 1895. Anatomie des Centres Nerveux, 1980, Masson ed. Rueff et Cie, Paris.

Dickson, J., Drury, H., Van Essen, D.C., 2001. 'The surface management system' (SuMS) database: a surface-based database to aid cortical surface reconstruction, visualization and analysis. Philos. Trans. R. Soc. London, Ser. B Biol. Sci. 356, 1277–1292.

Drenhaus, U., Schingnitz, G., Dorka, M., 1986. A method for a quantitative determination of changes in tissue volume as a result of perfusion fixation. Anat. Anz. 161, 327–332.

Economo, C.V., 1927. L'Architecture Cellulaire Normale De L'Ecorce Cerebrale. Masson and Cie, Paris.

Felleman, D.J., Van Essen, D.C., 1991. Distributed hierarchical processing in the primate cerebral cortex. Cereb. Cortex 1, 1–47.

Filipek, P.A., Kennedy, D.N., Boustany, R.M., Caviness Jr., V.S., 1988. Quantitative magnetic resonance imaging in late infantile neuronal ceroid lipofusionosis [abstract]. 17th Annual Meeting of the Child Neurology Society. Halifax, Nova Scotia.

Filipek, P.A., Richelme, C., Kennedy, D.N., Caviness Jr., V.S., 1994. The young adult human brain: an MRI-based morphometric analysis. Cereb. Cortex 4, 344–360.

Fischl, B., Dale, A.M., 2000. Measuring the thickness of the human cerebral cortex from magnetic resonance images. Proc. Natl. Acad. Sci. U. S. A. 97, 11050–11055.

Fischl, B., Sereno, M.I., Dale, A.M., 1999a. Cortical surface-based analysis: II. Inflation, flattening, and a surface-based coordinate system. NeuroImage 9, 195–207.

Fischl, B., Sereno, M.I., Tootell, R.B., Dale, A.M., 1999b. High-resolution intersubject averaging and a coordinate system for the cortical surface. Hum. Brain Mapp. 8, 272–284.

Gold, B.T., Balota, D.A., Cortese, M.J., Sergent-Marshall, S.D., Snyder, A.Z., Salat, D.H., Fischl, B., Dale, A.M., Morris, J.C., Buckner, R.L., 2005. Differing neuropsychological and neuroanatomical correlates of abnormal reading in early-stage semantic dementia and dementia of the Alzheimer type. Neuropsychologia 43, 833–846.

Hendry, S.H., Schwark, H.D., Jones, E.G., Yan, J., 1987. Numbers and proportions of GABA-immunoreactive neurons in different areas of monkey cerebral cortex. J. Neurosci. 7, 1503–1519.

Hofman, M.A., 1989. On the evolution and geometry of the brain in mammals. Prog. Neurobiol. 32, 137–158.

Igarashi, S., Kamiya, T., 1972. Atlas of the Vertebrate Brain: Morphological Evolution from Cyclostomes to Mammals. University of Tokyo Press, Tokyo.

Jones, E., 1981. Anatomy of the cerebral cortex: columnar input-output organization. In: Schmitt Jr., F., Worden, F., Adelman, G., Dennis, S. (Eds.), The Organization of the Cerebral Cortex. MIT Press, Cambridge, MA.

Jones, E., 1983. The columnar basis of cortical circuitry. The Clinical Neurosciences, vol. 5. Churchill-Livingstone, London, pp. 257–383.

Jones, E., 1990. Modulatory events in the development and evolution of the primate neocortex. In: Jones, E., Peters, A. (Eds.), Cerebral Cortex: Comparative Structure and Evolution of Cerebral Cortex: Part I. Plenum, New York.

Kennedy, D.N., Lange, N., Makris, N., Bates, J., Meyer, J., Caviness Jr., V.S., 1998. Gyri of the human neocortex: an MRI-based analysis of volume and variance. Cereb. Cortex 8, 372–384.

Kim, J.S., Singh, V., Lee, J.K., Lerch, J., Ad-Dab'bagh, Y., MacDonald, D., Lee, J.M., Kim, S.I., Evans, A.C., 2005. Automated 3-D extraction and evaluation of the inner and outer cortical surfaces using a Laplacian map and partial volume effect classification. NeuroImage 27, 210–221.

Luders, E., Narr, K.L., Thompson, P.M., Rex, D.E., Jancke, L., Steinmetz, H., Toga, A.W., 2004. Gender differences in cortical complexity. Nat. Neurosci. 7, 799–800.

Luders, E., Narr, K.L., Thompson, P.M., Rex, D.E., Jancke, L., Toga, A.W., 2005a. Hemispheric asymmetries in cortical thickness. Cereb. Cortex (Electronic publication ahead of print).

Luders, E., Thompson, P.M., Narr, K.L., Toga, A.W., Jancke, L., Gaser, C., 2005b. A curvature-based approach to estimate local gyrification on the cortical surface. NeuroImage (Electronic publication ahead of print).

Luders, E., Narr, K.L., Thompson, P.M., Rex, D.E., Woods, R.P., Deluca, H., Jancke, L., Toga, A.W., 2005c. Gender effects on cortical thickness and the influence of scaling. Hum. Brain Mapp. (Electronic publication ahead of print).

Makris, N., Meyer, J.W., Bates, J.F., Caviness Jr., V.S., Kennedy, D.N., 1999. MRI-based topographic parcellation of human cerebral white matter and nuclei: II. Rationale and applications with systematics of cerebral connectivity. NeuroImage 9, 17–45.

Makris, N., Hodge, S.M., Haselgrove, C., Kennedy, D.K., Dale, A.M., Fischl, B., Rosen, B.R., Harris, G., Caviness, V.S.J., Schmahmann, J.D., 2003. Human cerebellum: surface-assisted cortical parcellation and volumetry with magnetic resonance imaging. J. Cogn. Neurosci. 15, 1–16.

Makris, N., Schlerf, J.E., Hodge, S.M., Haselgrove, C., Albaugh, M.D., Seidman, L.J., Rauch, S.L., Harris, G., Biederman, J., Caviness Jr., V.S., Kennedy, D.N., Schmahmann, J.D., 2005. MRI-based surface-assisted parcellation of human cerebellar cortex: an anatomically specified method with estimate of reliability. NeuroImage 25, 1146–1160.

Meyer, J., Makris, N., Bates, J., Caviness, V.S. Jr., Kennedy, D.N., 1999. MRI-Based topographic parcellation of the human cerebral white matter: I. Technical foundations. NeuroImage 9, 1–17.

Mountcastle, V., 1998. Perceptual Neuroscience: The Cerebral Cortex. Harvard University Press, Cambridge, MA.

Mouritzen Dam, A., 1979. Shrinkage of the brain during histological procedures with fixation in formaldehyde solutions of different concentrations. J. Hirnsforsch. 20, 115–119.

Narr, K.L., Toga, A.W., Szeszko, P., Thompson, P.M., Woods, R.P., Robinson, D., Sevy, S., Wang, Y., Schrock, K., Bilder, R.M., 2005. Cortical thinning in cingulate and occipital cortices in first episode schizophrenia. Biol. Psychiatry 58, 32–40.

O'Kusky, J., Colonnier, M., 1982. A laminar analysis of the number of neurons, glia, and synapses in the adult cortex (area 17) of adult macaque monkeys. J. Comp. Neurol. 210, 278–290.

Ono, M., Jubik, S., Abernathy, C.D., 1990. Atlas of the Cerebral Sulci. Thieme Verlag, New York.

Pakkenberg, B., Gundersen, H.J., 1997. Neocortical neuron number in humans: effect of sex and age. J. Comp. Neurol. 384, 312–320.

Papez, J.W., 1929. Comparative Neurology. Hafner Publishing Co, New York.

Prothero, J.W., Sundsten, J.W., 1984. Folding of the cerebral cortex in mammals. A scaling model. Brain Behav. Evol. 24, 152–167.

Purves, D., 1988. Body and Brain: A Trophic Theory of Neural Connections. Harvard Univ. Press, Cambridge.

Rademacher, J., Galaburda, A.M., Kennedy, D.N., Filipek, P.A., Caviness, V.S.J., 1992. Human cerebral cortex: localization, parcellation, and morphometry with magnetic resonance imaging. J. Cogn. Neurosci. 4, 352–374.

Rakic, P., 1972. Mode of cell migration to the superficial layers of fetal monkey neocortex. J. Comp. Neurol. 145, 61–83.

Rakic, P., 1974. Neurons in rhesus monkey visual cortex: systematic relation between time of origin and eventual disposition. Science 183, 425–427.

Rakic, P., 1975. Role of cell interaction in development of dendritic patterns. Adv. Neurol. 12, 117–134.

Rakic, P., 1977. Prenatal development of the visual system in rhesus monkey. Philos. Trans. R. Soc. London, B 278, 245–260.

Rakic, P., 1978. Neuronal migration and contact guidance in the primate telencephalon. Postgrad. Med. J. 54 (Suppl. 1), 25–40.

Rakic, P., 1982. Early developmental events: cell lineages, acquisition of neuronal positions, and areal and laminar development. Neurosci. Res. Program Bull. 20, 439–451.

Rakic, P., 1988. Specification of cerebral cortical areas. Science 241, 170–176.

Rakic, P., 1990. Principles of neural cell migration. Experientia 46, 882–891.

Rakic, P., 1990. Radial unit hypothesis of cerebral cortical evolution. In: Eccles Jr, J., Creutzfeldt, O. (Eds.), Principles and Design and Operation of the Brain. Pontificae Academiae Scripta Varia, Vatican City.

Rakic, P., 1995. A small step for the cell, a giant leap for mankind: a hypothesis of neocortical expansion during evolution. Trends Neurosci. 18, 383–388.

Rockel, A.J., Horns, R.W., Powell, T.P.S., 1980. The basic uniformity of structure of the neocortex. Brain 103, 221–244.

Romeis, B., 1968. Mikroskopische Technik. Oldenbourg Verlag, Munchen.

Salat, D.H., Buckner, R.L., Snyder, A.Z., Greve, D.N., Desikan, R.S., Busa, E., Morris, J.C., Dale, A.M., Fischl, B., 2004. Thinning of the cerebral cortex in aging. Cereb. Cortex 14, 721–730.

Schuz, A., Palm, G., 1989. Density of neurons and synapses in the cerebral cortex of the mouse. J. Comp. Neurol. 286, 442–455.

Smith, S.M., Jenkinson, M., Woolrich, M.W., Beckmann, C.F., Behrens, T.E., Johansen-Berg, H., Bannister, P.R., De Luca, M., Drobnjak, I., Flitney, D.E., Niazy, R.K., Saunders, J., Vickers, J., Zhang, Y., De Stefano, N., Brady, J.M., Matthews, P.M., 2004. Advances in functional and structural MR image analysis and implementation as FSL. NeuroImage 23 (Suppl. 1), S208–S219.

Stephan, H., 1960. Methodische Studien Uber den quantitativen Vergleich architektonischer Struktureinheiten des menschlichen Gehirns. Z. Wiss. Zool. 164, 1–2.

Takahashi, T., Nowakowski, R.S., Caviness Jr., V.S., 1996a. Interkinetic and migratory behavior of a cohort of neocortical neurons arising in the early embryonic murine cerebral wall. J. Neurosci. 16, 5762–5776.

Takahashi, T., Nowakowski, R.S., Caviness Jr., V.S., 1996b. The leaving or Q fraction of the murine cerebral proliferative epithelium: a general model of neocortical neuronogenesis. J. Neurosci. 16, 6183–6196.

Talairach, J., Tournoux, P., 1988. Co-Planar Stereotaxic Atlas of the Human Brain. Thieme Medical Publishers, Inc., New York.

Talairach, J., Szikla, G., Tournoux, P., 1967. Atlas d'Anatomie Stereotaxique du Telencephale. Masson, Paris.

Thompson, P.M., Moussai, J., Zohoori, S., Goldkorn, A., Khan, A.A., Mega, M.S., Small, G.W., Cummings, J.L., Toga, A.W., 1998. Cortical variability and asymmetry in normal aging and Alzheimer's disease. Cereb. Cortex 8, 492–509.

Toga, A.W., 2002. Neuroimage databases: the good, the bad and the ugly. Nat. Rev., Neurosci. 3, 302–309.

Van Essen, D.C., 2005. A population-average, landmark- and surface-based (PALS) atlas of human cerebral cortex. NeuroImage 28, 635–662.

Van Essen, D.C., Drury, H.A., 1997. Structural and functional analyses of human cerebral cortex using a surface-based atlas. J. Neurosci. 17, 7079–7102.

Van Essen, D., Felleman, D., De Yoe, E., Olavarria, J., Knierim, J., 1990. Modular and Hierarchical organization of extrastriate visual cortex in the macaque monkey. Cold Spring Harbor Symp. Quant. Biol. 55, 679–696.

Van Essen, D.C., Drury, H.A., Joshi, S., Miller, M.I., 1998. Functional and structural mapping of human cerebral cortex: solutions are in the surfaces. Proc. Natl. Acad. Sci. U. S. A. 95, 788–795.

Welker, W., 1990. Why does cerebral cortex fissure and fold? A review of determinants of gyri and sulci. In: Jones, E.G., Peters, A. (Eds.), Cerebral Cortex: Comparative Structure and Evolution of Cerebral Cortex, Part II, Vol. 8B. Plenum Press, New York, pp. 3–136.

Werner, L., Winkelmann, E., 1976. Untersuchungen zur Struktur der thalamo-kortikale Projektionsneuronen and Interneuronen im Corpus geniculatum laterale pars dorsalis (Cgld) der Albinoratte nach unterschiedlicher histologischer Technik. Anat. Anz. Bd. 139, 142–157.

Wiegand, L.C., Warfield, S.K., Levitt, J.J., Hirayasu, Y., Salisbury, D.F., Heckers, S., Dickey, C.C., Kikinis, R., Jolesz, F.A., McCarley, R.W., Shenton, M.E., 2004. Prefrontal cortical thickness in first-episode psychosis: a magnetic resonance imaging study. Biol. Psychiatry 55, 131–140.

Worth, A.J., Makris, N., Caviness Jr., V.S., Kennedy, D.N., 1997a. Neuroanatomical segmentation in MRI: technological objectives. Int. J. Pattern Recogn. Artif. Intell. 11, 1161–1187.

Worth, A.J., Makris, N., Meyer, J.W., Caviness Jr., V.S., Kennedy, D.N., 1997b. Automated segmentation of brain exterior in MR images driven by empirical procedures and anatomical knowledge. International Conference on Information Processing in Medical Imaging. Poultney, Vermont.

Yeterian, E.H., Pandya, D.N., 1985. Corticothalamic connections of the posterior parietal cortex in the rhesus monkey. J. Comp. Neurol. 237, 408–426.

Zilles, K., 2005. Architecture of the human cerebral cortex. In: Paxinos, G., Mai, J. (Eds.), The Human Nervous System. Elsevier Academic Press, San Diego, pp. 997–1055.